Study on the Mechanical Characteristics of Concrete Pavement Corner Detachment and Grouting Reinforcement Using the FEM-DEM Coupling Approach

Xiaoyong Zhang[1], Baoyin Mei[1], Deqiang Chen[2], Jianxue Feng[3] and Tiancheng Wang[4,*]

[1] Department of Architectural Engineering, Guizhou Communications Polytechnic University, Guiyang, 551400, China

[2] Guangxi Beitou Transportation Maintenance Technology Group Co., Ltd., Nanning, 530022, China

[3] School of Civil Engineering and Architecture, Guizhou Minzu University, Guiyang, 550025, China

[4] Key Laboratory of Geotechnical Mechanics and Engineering of Ministry of Water Resources, Changjiang River Scientific Research Institute, Wuhan, 430010, China

INFORMATION

Keywords:
Cement concrete pavements
FEM-DEM coupling method
mesoscopic parameters
crack distribution
force chain

DOI: 10.23967/j.rimni.2025.10.68073

SCIPEDIA Revista Internacional de Métodos Numéricos para Cálculo y Diseño en Ingeniería

Revista Internacional Métodos numéricos para cálculo y diseño en ingeniería RIMNI

In cooperation with CIMNE

Study on the Mechanical Characteristics of Concrete Pavement Corner Detachment and Grouting Reinforcement Using the FEM-DEM Coupling Approach

Xiaoyong Zhang[1], Baoyin Mei[1], Deqiang Chen[2], Jianxue Feng[3] and Tiancheng Wang[4,*]

[1]Department of Architectural Engineering, Guizhou Communications Polytechnic University, Guiyang, 551400, China

[2]Guangxi Beitou Transportation Maintenance Technology Group Co., Ltd., Nanning, 530022, China

[3]School of Civil Engineering and Architecture, Guizhou Minzu University, Guiyang, 550025, China

[4]Key Laboratory of Geotechnical Mechanics and Engineering of Ministry of Water Resources, Changjiang River Scientific Research Institute, Wuhan, 430010, China

ABSTRACT

Cement concrete pavements have significant advantages in the construction of transportation infrastructure. However, the disease of slab bottom voids affects their performance and service life. In this study, the Finite Element Method-Discrete Element Method (FEM-DEM) coupling method was used to deeply explore the mechanical characteristics of concrete pavement corner voids and grouting reinforcement. First, a discrete element model for corner voids was constructed, and uniaxial compression simulations were carried out to calibrate the mesoscopic parameters of the concrete surface layer and the base course. Subsequently, an FEM-DEM coupling model was established to simulate the mechanical responses of the pavement slab under different working conditions. The research found that when there is a corner void, the cracking load is 75 kN, and the peak load is 96.8 kN. After exceeding the peak load, the cracks expand rapidly. When the strain reaches 0.2, the crack growth slows down. The displacement expands in a triangular shape, and the failure mode is shear failure. After grouting reinforcement, the peak strength increases by 53% to 150 kN, the cracking pressure is 75 kN, the cracks expand rapidly first and then stabilize, and the failure form is rectangular. In addition, the load transfer, crack distribution, force chain distribution, etc., show different laws in the void and reinforced states. The FEM-DEM model overcomes traditional numerical limits, precisely simulating structure-void interactions and reinforcing mechanics. It fills a meso-macro research gap, offering new insights for pavement engineering and supporting corner void grouting treatments.

OPEN ACCESS

Received: 20/05/2025

Accepted: 18/07/2025

Published: 15/12/2025

DOI
10.23967/j.rimni.2025.10.68073

Keywords:
Cement concrete pavements
FEM-DEM coupling method
mesoscopic parameters
crack distribution
force chain

*Correspondence: Tiancheng Wang (xibianxiaocheng@126.com).

1 Introduction

Cement concrete roads exhibit significant advantages in the realm of transportation infrastructure construction. It's good water stability results from the dense microstructure formed after setting and hardening, which effectively prevents moisture penetration and mitigates water-related damages [1]. Regarding flexural performance, the material properties and optimal mix design create a high-strength, rigid structure capable of uniformly dispersing loads under external forces, minimizing deformation and crack formation [2]. Although its rigidity is substantial, on poor subgrades, appropriate design and construction measures, including base layer placement and steel bar reinforcement, enable it to adapt to subgrade deformations. Reinforcement with steel improves the overall integrity and toughness of the structure, enabling it to withstand tensile stresses during subgrade settlement and restricting crack propagation. Leveraging these superior properties, more countries globally are actively developing cement concrete roadways to address transportation demands and enhance infrastructure quality [3,4]. Common defects in concrete pavements include misalignment, cracks, fragmentation, and voids, with misalignment, cracks, and fragmentation being closely related to hollowing of the slab bottom [5,6].

Under the repeated action of vehicle loads, the subbase beneath the concrete pavement will undergo cumulative plastic deformation, leading to the formation of voids between the concrete pavement and the subbase, i.e., local hollowing beneath the slab [7]. Additionally, due to the nonlinear temperature distribution within the slab, the slab warps upwards or downwards, accelerating the separation between the slab and the foundation, resulting in hollowing at the bottom of the slab. Hollowing creates a pathway for water infiltration [8]. If pavement joints or cracks are not maintained in time, rainwater can enter the subbase from these joints or cracks, forming water accumulation. The accumulated water mixes with fine particles in the subbase to create slurry, which splashes along the joints of the slab, causing mud-pumping damage, which in turn accelerates the progression of bottom slab hollowing. The concrete slab at the hollowing position acts like a cantilever, experiencing significant stress and bending deflection under vehicle loads. With repeated vehicle loading, this leads to eventual fracture [9].

In actual engineering, understanding the mechanism of bottom slab hollowing and the changes in macromechanical properties after hollowing is essential for developing effective preventive and corrective measures [10]. Grouting refers to a technique where a solidifiable liquid substance is injected into rock fractures via a grouting pump or similar equipment, aiming to enhance the physical and mechanical attributes of fractured rock masses [11]. Engineering applications have demonstrated that this approach efficiently boosts the strength, structural integrity, and stability of fractured rock formations. In recent years, numerous researchers have conducted fruitful investigations into grouting materials, leading to the development of various types with distinct properties [12]. These materials can be categorized primarily into inorganic cementitious grouts and organic chemical grouts. However, there is no research on the mechanical state after grouting treatment for bottom slab hollowing in road pavement, and the study of grouting treatment methods for bottom slab hollowing lacks a mechanical foundation, which to some extent limits the development and practical application of this method [13].

Concrete grouting reinforcement, relying on the trinity repair mechanism of "filling densification-extrusion reinforcement-curing enhancement", has become the preferred technology for treating pavement voids and foundation defects [14]. This technology injects cement-based grout under high pressure, allowing the grout to penetrate into void areas and cracks. Compared with other methods, its comprehensive cost is much lower than that of polymer grouting, and it is more suitable for long-term load requirements. While tie bars require large-area excavation and cannot radically cure voids,

polymer grouting is minimally invasive and quick-setting but has high costs and low modulus, and carbon fiber cloth is only suitable for surface cracks with high cost. Therefore, for large-area void diseases, cement grouting has significant advantages in cost performance, structural restoration, and application scope [15].

Difficulties in implementation and technical challenges include insufficient accuracy in void detection, as traditional visual inspection methods (such as observing mud pumping and slab warping) and deflection meter detection (determining voids when the deflection value >0.2 mm) have subjective errors with a missed detection rate of up to 15%–20%, while advanced equipment like Ground Penetrating Radar (GPR) and Falling Weight Deflectometer (FWD), though capable of accurately locating void areas, has a high single detection cost of 50,000–80,000 RMB per kilometer, requires professional operators, and has a popularity rate of less than 30% in local highway maintenance; there are also difficulties in grouting process control, such as uneven slurry distribution where cement-based slurry is prone to form "table-leg support" (local concentrated support) due to insufficient fluidity, leading to stress concentration and new cracks, as seen in the Beijing-Guangzhou High-Speed Railway case where 23% of the repaired slabs developed radial cracks for this reason, and difficulty in ensuring lifting accuracy where a pressure exceeding 1.5 MPa may disturb the base course while insufficient pressure cannot fill microcracks, with actual construction requiring dynamic pressure adjustment (recommended 0.8–1.5 MPa) but 30% of projects experiencing slab corner warping due to pressure out of control. In terms of cost-effectiveness and engineering feasibility, polymer grouting, despite its short construction period (with an 80% increase in construction efficiency), has a material cost 6–8 times that of cement slurry, making it less feasible for local highway projects with limited budgets. Long-term durability issues involve material performance degradation, including poor water stability where cement-based grout is prone to $Ca(OH)_2$ leaching under rainwater infiltration, resulting in a 30%–40% strength attenuation and accelerating base course loosening (such as secondary voids in the backfilled soil section in the Dongdingzhou case), and temperature sensitivity where cement slurry hardens slowly at low temperatures (<5°C) and its fluidity drops sharply at high temperatures, leading to a narrow construction window, in contrast to polymer grouting which can be operated at −20°C–60°C; there are also structural synergy defects like interlayer bond failure due to modulus mismatch between the grouting body and the original base course, easily causing interface shear cracks under heavy traffic loads, and insufficient fatigue life where grouting-repaired slabs, under design loads, have a crack development rate 2.3 times that of non-void slabs within 5 years, mainly due to stress concentration caused by residual micro-voids in the void areas.

In 1979, Cundall and Hart [16] introduced the discrete element method suitable for soil mechanics. Discrete Element Method (DEM) divides the computational time into sufficiently small steps and applies Newton's second law and the force-displacement law at each step. The basic unit of PFC is the particle, which gives it a clear advantage in simulating cracking, fragmentation, and other failure behaviors. The discrete element method is one of the commonly employed methods for studying the performance of pavement materials. Pei et al. [17] developed a discrete element model for the development of reflective cracks in cement pavement with an asphalt overlay. Under bending and shear loads, an increase in the thickness of the asphalt overlay can suppress the development of reflective cracks, while the interlayer bonding strength has little impact on crack development. Bending loads are more effective in promoting crack development than shear loads. Vaddy et al. [18] used DEM to simulate the flexural performance of pervious concrete and performed calibration and validation of the simulation model. Xie et al. [19] applied the DEM to investigate the effects of geometric structure cutting on transverse crack management and proposed strategies tailored to geometric structure cutting. Zhu et al. [20] employed the DEM to investigate the propagation of reflective cracks under

moving loads with varying bonding conditions, identifying a three-stage progression of cracks from the base to the pavement, which includes rapid extension, stable growth, and failure. The DEM serves as a powerful numerical approach for simulating crack propagation and wear in granular materials. However, the high computational cost of DEM restricts its application to large-scale domains. To tackle this challenge, we utilize DEM to model regions undergoing crack propagation and wear, while employing the Finite Element Method (FEM) for areas with minor deformations. This strategy effectively reduces the computational load [21]. Jin et al. [22] established three-dimensional transient dynamic models of two typical rippers cutting RC piles based on the FEM-DEM coupling method, described the mechanical behavior of concrete via DEM, considered the influence of steel bars via FEM, and analyzed the damage characteristics of steel bars and concrete as well as the force patterns of rippers. Ge et al. [23] developed a novel FEM-DEM coupling framework to precisely assess particle-scale responses of asphalt mixture layers under realistic non-uniform tire loads, including free rolling and full braking conditions.

This study focuses on the issue of microcracking in concrete pavements. It is difficult to study full-scale road structures using PFC, as the boundary wall units in PFC are rigid, which does not accurately represent real-world conditions [24]. Therefore, it can be seen that the continuous-discrete coupling method effectively combines the advantages of the discrete element method and finite element (or finite difference) method. This method is widely used in various fields and is a rational and efficient approach in numerical simulations [25]. The FEM-DEM coupling method is employed to simulate processes such as compression and fracture in concrete pavements by defining bonding and particle morphology, investigating the micro-damage characteristics of concrete pavements. A parallel bonding model is used to substitute concrete, and the concrete damage characteristics are explored by constructing a micro-scale DEM model [26].

This study uses the FEM-DEM coupling method to compare the behavior of concrete pavement corner delamination and post-grouting reinforcement. First, uniaxial compression simulations were performed to calibrate the mesoscopic parameters of the concrete surface and base layers. A FEM-DEM coupling model of the pavement structure was developed, and a comparative analysis was conducted on macroscopic mechanical characteristics as well as mesoscopic changes such as particle displacement, force chains, and crack propagation, both before and after grouting reinforcement of corner delamination. The findings offer a theoretical foundation for the development of grouting treatment methods for corner delamination in concrete pavements.

2 Development and Mesoscopic Parameter Calibration of the DEM Model for Pavement Slab Corner Void

2.1 Computational Model

The calculation model for the bottom voiding of the concrete pavement is illustrated in Fig. 1. The concrete panel has a length of 5 m, a width of 4 m, and a thickness of 0.26 m. The base layer is 0.5 m thick, and the foundation is expanded to dimensions of 7 m × 6 m × 6 m. The voiding area is positioned at the bottom of the concrete panel, with dimensions of 1 m × 1 m × 0.01 m. The primary calculation parameters for each structural layer are provided in Table 1.

A single wheel load is chosen with an area of 20 cm × 20 cm, and the spacing between the two wheels is 30 cm. By calculating and comparing different load positions, it is observed that when grouting is applied to the edge of the pavement panel, the wheel load has the most detrimental effect when applied symmetrically to the bottom plate on one side of the panel. Furthermore, the load is most

damaging when applied to the corner of the pavement panel. The loading configuration is shown in Fig. 2.

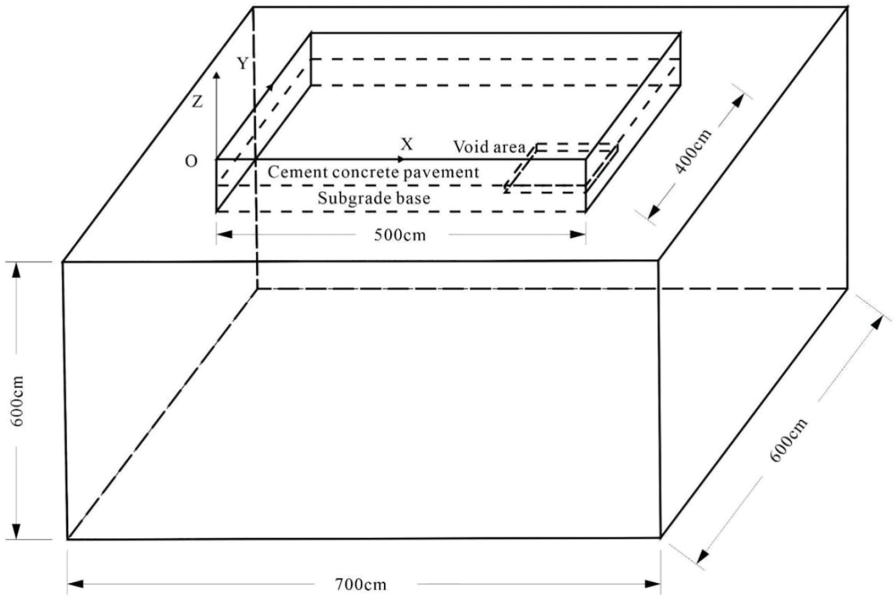

Figure 1: Computational model of pavement slab corner void

Table 1: Key calculation parameters for each structural layer

Structural layers	Thickness (cm)	Young's modulus E (MPa)	Poisson's ratio
Concrete slab	26	30,000	0.15
Grouted block	1	1000	0.25
Sub-base	50	1200	0.20
Ground subgrade	–	300	0.40

2.2 Principle of Continuous-Discrete Coupling Method

The coupled numerical model consists of three parts: the DEM model, the FEM model, and the coupling wall. The numerical simulation diagram is shown in Fig. 3. The coupling wall is attached to the surface of the FEM model elements, and its vertices coincide with the element grid points. As the interface connecting the DEM model and the FEM model, the coupling wall ensures the interactive transmission of force information (force and torque) and displacement information (velocity and position) between the two models through the interface, thereby realizing the discrete-continuous coupling scheme. The DEM model transmits force information to the vertices of the coupling wall through contact points, and the FEM model receives the force information from the vertices of the coupling wall, and then updates the displacement information to the DEM model along the original path. In coupled simulations, when using discrete element modeling for macroscopic engineering, the number of particles required is enormous, making the calculations time-consuming and labor-intensive. The continuous-discrete coupling method can partially solve this problem by leaving an

empty zone in the core of the continuous element part, within which discrete element modeling is employed. The interaction between continuous and discrete elements occurs via an interface, thus achieving a balance between computational efficiency and precision.

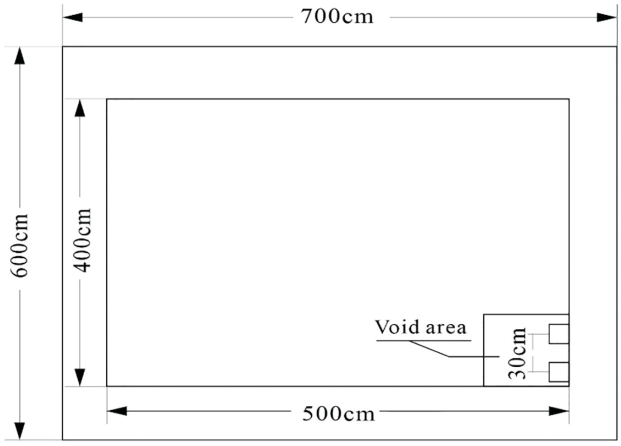

Figure 2: Computational load arrangement for pavement slab corner void

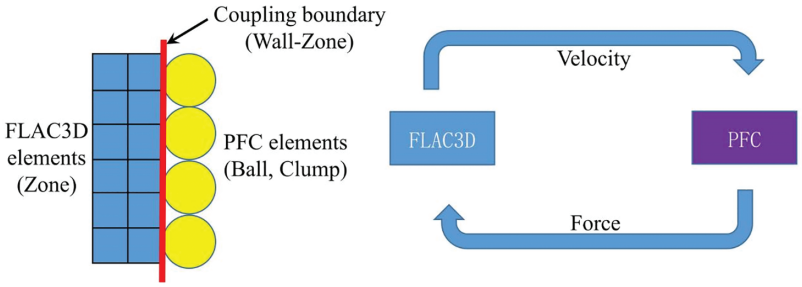

Figure 3: The principle of FEM-DEM coupling

2.3 Calibration of Discrete Element Mesoscopic Parameters

In discrete element modeling, the macroscopic mechanical properties of materials are determined by the mesoscopic parameters of particles and the contact constitutive models [8]. This study employs uniaxial compression tests to determine the physical and mechanical properties of the discrete element model. This research uses standard concrete cubes with dimensions of 100 mm × 100 mm × 100 mm for conducting uniaxial compression tests. In the uniaxial compression tests, a displacement-controlled loading mode is used to apply the load by accurately controlling the displacement changes, ensuring the reliability and accuracy of the test data. The experimental model of the standard concrete specimen and the discrete element model are shown in Fig. 4, laying the foundation for subsequent in-depth numerical analysis and mechanical performance studies.

The particle size and mesoscopic parameters of the uniaxial specimen are the same as those of the foundation. Rigid wall boundaries (wall) are used as the upper and lower loading plates, with a loading rate of 0.01 mm/s. The normal and tangential contact stiffness match the specimen's stiffness. After multiple trial calculations, the mesoscopic parameters are as shown in Table 2, and the stress-strain curves of different models are as shown in Figs. 5 and 6.

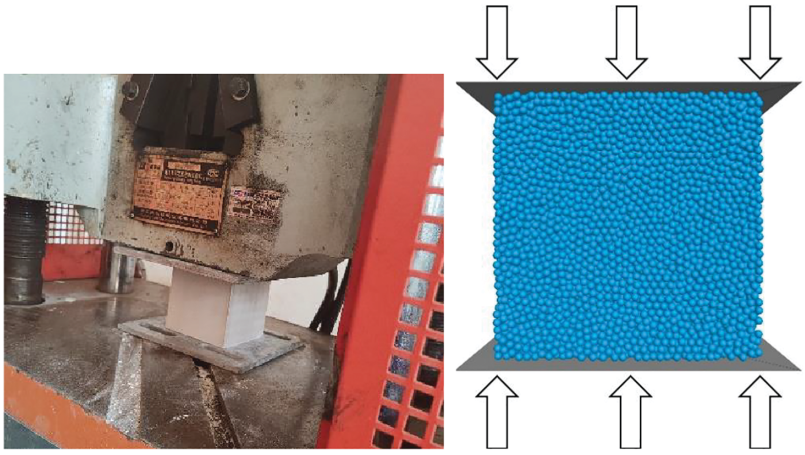

(a) (b)

Figure 4: Simulation of uniaxial compression using discrete element method: (a) concrete sample; (b) Schematic diagram of uniaxial compression discrete element

Table 2: Mesoscale parameters for various geological layers

Different strata	Cement concrete pacement	Subgrade base
Particle contact model	Linearpbond	
Effective modulus (Pa)	50e9	1e9
Normal-to-shear stiffness ratio	1	1
Bond effective modulus (Pa)	50e9	1e9
Bond normal-to-shear stiffness ratio	1	1
Tensile strength (N)	15e6	11.2e5
Cohesion (N)	15e6	11.2e5
Friction angle (°)	0	10
Friction coefficient	0.5	0.3
Particle density (kg/m^3)	2800	2800

Comparison and validation between DEM and lboratory tests in the research on the concrete surface layer, uniaxial compression tests were conducted both through DEM simulations and laboratory experiments, yielding the corresponding stress-strain curves as shown in the Fig. 5. A comparative analysis of the curve profiles reveals a high degree of consistency between the DEM simulation curve and the laboratory test curve. During the stress development phase, both curves exhibit a similar pattern: stress increases progressively with strain, reaches a peak value, and then declines. Focusing specifically on the peak strength, both the laboratory tests and DEM simulations yield a value of approximately 30 MPa, demonstrating excellent numerical agreement. This consistency strongly validates the rationality and effectiveness of the mesoscopic parameters employed in the DEM simulations. In DEM modeling, mesoscopic parameters are fundamental for constructing the model and accurately representing the material's mechanical behavior. The close match between the simulation results and the actual laboratory test data, particularly in such a critical mechanical

peak strength and the overall curve trend, indicates that these parameters can precisely capture the mechanical response characteristics of the concrete surface layer under uniaxial compression. Consequently, they provide a reliable data foundation and parameter basis for subsequent DEM-based simulations under more complex conditions, enabling in-depth investigations into the evolution of the concrete surface layer's mechanical properties under various conditions.

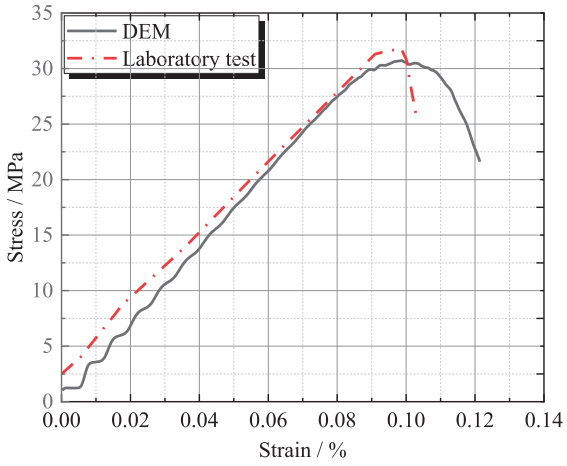

Figure 5: Stress-strain curve of the concrete surface layer

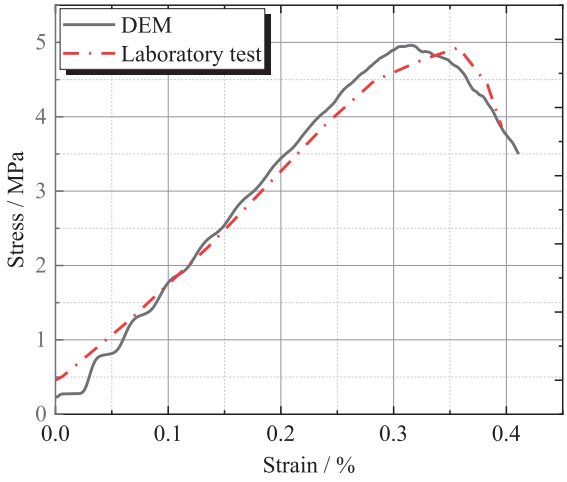

Figure 6: Stress-strain curve of the base layer

For the base layer, stress-strain curves from DEM simulation and lab uniaxial compression test are shown in the Fig. 6. As strain rises from 0, both curves DEM: solid line; dashed line show stress increasing, reflecting internal force mobilization under compression. Both DEM and lab tests give a peak strength of 5 MPa, with peak strain at 0.32%. This high consistency validates the rationality of mesoscopic parameters in DEM.

2.4 Establishment of the FEM-DEM Coupling Model

The FEM-DEM coupled model for the bottom void of the concrete pavement is shown in Fig. 7. The subgrade consists of particles with a radius of 3 cm, and the concrete slab consists of particles

with a radius of 2.5 cm. The model is composed of a large number of particles, totaling 125,900, with 59,587 particles in the concrete surface layer and 66,314 particles in the subgrade. This model is developed using the DEM and requires validation before use to ensure its reliability for further research. Choosing the appropriate particle radius ensures the accuracy of the simulation results. A larger particle radius reduces computation time but may ignore some microscopic mechanical behaviors, while a smaller radius provides more accurate simulation of micro-mechanical behaviors at the cost of increased computational cost [27–29]. The DEM is used to simulate the behavior of granular materials, reflecting the mechanical properties of the material through particle interactions. The subgrade is modeled with a finite element mesh, which helps improve computational efficiency [30]. The parameters are shown in Table 3. The FEM-DEM coupling method combines the benefits of the FEM and the PFC. The FEM is advantageous for continuous media and large deformation problems, while the DEM is excellent for simulating granular materials and crack propagation. This coupled method enables a more comprehensive simulation of complex geotechnical engineering problems [31,32].

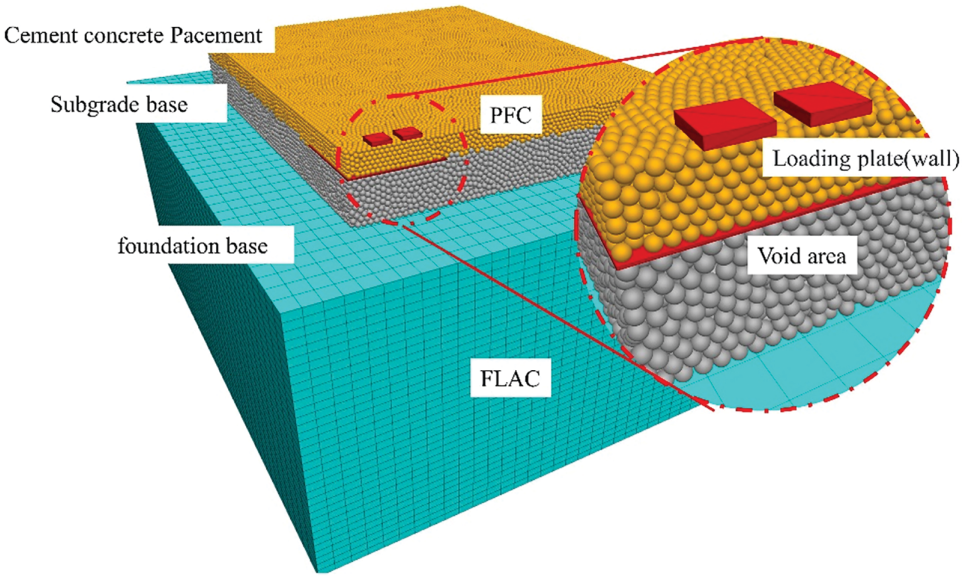

Figure 7: FEM-DEM coupled numerical model of pavement slab corner void

Table 3: FEM parameters of the subgrade

Structural Layers	Model	Density (kg/m^3)	Young's modulus (MPa)	Poisson's ratio	Bulk modulus (MPa)	Shear modulus (MPa)
Subgrade	Linear elastic model	2300	300	0.4	500	107.4

The establishment of the void model employs an efficient approach. Initially, a wall is created in the void region. The role of this wall is to maintain the model's stability at the initial stages of model setup. Once the model reaches equilibrium and appropriate microscopic parameters are assigned, the

wall is deleted to create the void region. The benefit of this approach is that after the model achieves equilibrium, the wall is removed to create the void region. At this stage, the model is stable, allowing for further calculations to be carried out based on this stability, thus reducing the number of iterations and computational load.

This paper uses a rigid wall (wall) as the loading plate for the subgrade model. Based on the research results of Zhang et al. [29], after several trial calculations, a loading rate of 0.005 mm/s was determined. This speed guarantees that the model undergoes quasi-static loading during the loading process, thus optimizing computational efficiency. The table of contact models for the FEM-DEM coupled numerical model of voids at the corner of the pavement slab is shown in Table 4.

Table 4: Contact models for the FEM-DEM coupled numerical model of voids at the corner of pavement slab

Material	Cement concrete pacemen	Subgrade base	Foundation base	Cement concrete pacemen-subgrade base	Subgrade base-foundation base
Contact model	Linearpbond	Linearpbond	Linear elastic model	Linear elastic model	Linear

Fig. 8 shows displacement contour plot and force chain distribution of the DEM model after self-weight equilibrium. As shown in the figure, it can be observed that the settlement displacement is primarily distributed horizontally. This phenomenon is consistent with the characteristic of uniform compression of the soil in the vertical direction under the influence of gravity. The force chain is densely distributed at the lower part and sparsely distributed at the upper part. This distribution pattern is in line with the initial stress distribution of the actual soil under the influence of gravity.

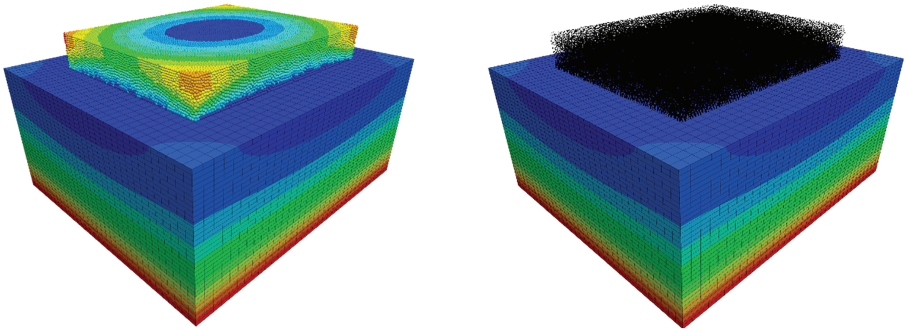

(a) (b)

Figure 8: Gravity equilibrium of the discrete element model of the subgrade: (a) Displacement contour map; (b) Contact force chain distribution map

3 Analysis of DEM Results

3.1 Analysis of Simulation Results for Pavement Slab Bottom Void

Fig. 9 shows load and microcrack evolution vs. displacement for the pavement slab corner void under loading. From the figure, it can be observed that in the case of corner detachment, the change

in contact force and crack number with displacement follows a specific pattern. The initiation load is 75 kN, which is the critical point at which microcracks start to form. Before the initiation load, the internal stress of the concrete structure is primarily supported by the material's elastic modulus, and the stress has not yet reached the level needed to generate microcracks. When the load reaches the peak of 96.8 kN, the number of cracks is 179. This shows that before the peak load, despite the continuous increase in load, the formation and propagation of microcracks are relatively slow. This is due to the fact that in the early stages of loading, there are fewer stress concentration zones within the concrete, and the formation and propagation of microcracks are limited by the surrounding uncracked concrete. As displacement increases, after surpassing the peak load, the number of cracks increases rapidly. This occurs because, after exceeding the peak load, the stress concentration in the concrete intensifies, leading to the rapid expansion of existing microcracks and the formation of new ones. When the strain reaches 0.2, the crack growth rate slows down. This could be because, at this strain level, a relatively stable crack network has formed within the concrete, limiting the formation of new cracks due to the existing network. At this point, the load is primarily supported by the existing crack network and the uncracked concrete part, causing the increase in crack numbers to slow down.

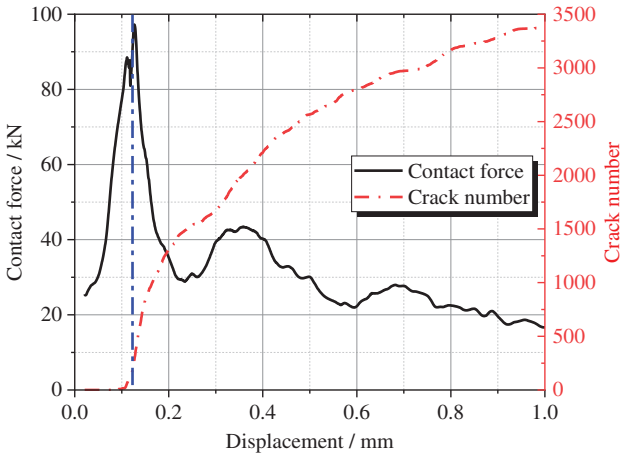

Figure 9: Load and microcrack evolution vs. displacement for the pavement slab corner void under loading

The displacement contour plot of the pavement slab corner void under loading is shown in Fig. 10. From this diagram, it can be observed that the displacement region extends outward from beneath the loading plate. During this process, the displacement growth pattern follows a triangular shape. When the displacement is small, it is primarily concentrated beneath the loading plate, with a tendency to spread outward. With the increase in load, the triangular displacement expansion pattern gradually becomes more defined. This displacement expansion pattern is likely caused by the presence of corner detachment, which alters the load transfer path. The displacement mainly extends along the edges of the detachment area and below the loading plate, forming a triangular shape. The displacement contour diagram clearly shows that the failure mode is shear failure. Once the displacement reaches a certain level, the failure surface appears on both sides of the detachment area. The mechanism of shear failure is that the shear stress generated within the concrete under load exceeds its shear strength. In the case of corner detachment, the concrete on both sides of the detachment area experiences significant shear stress. This is due to the severe stress concentration at the edges of the detachment area during the load transfer process, which causes the shear stress in that area to increase rapidly. When the shear

stress reaches the shear strength of the concrete, shear bands will form on both sides of the detachment area, resulting in the failure of the concrete structure. This failure mode is of great significance in real-world engineering, as shear failure often leads to the sudden collapse of concrete structures, impacting the safety and durability of the structure.

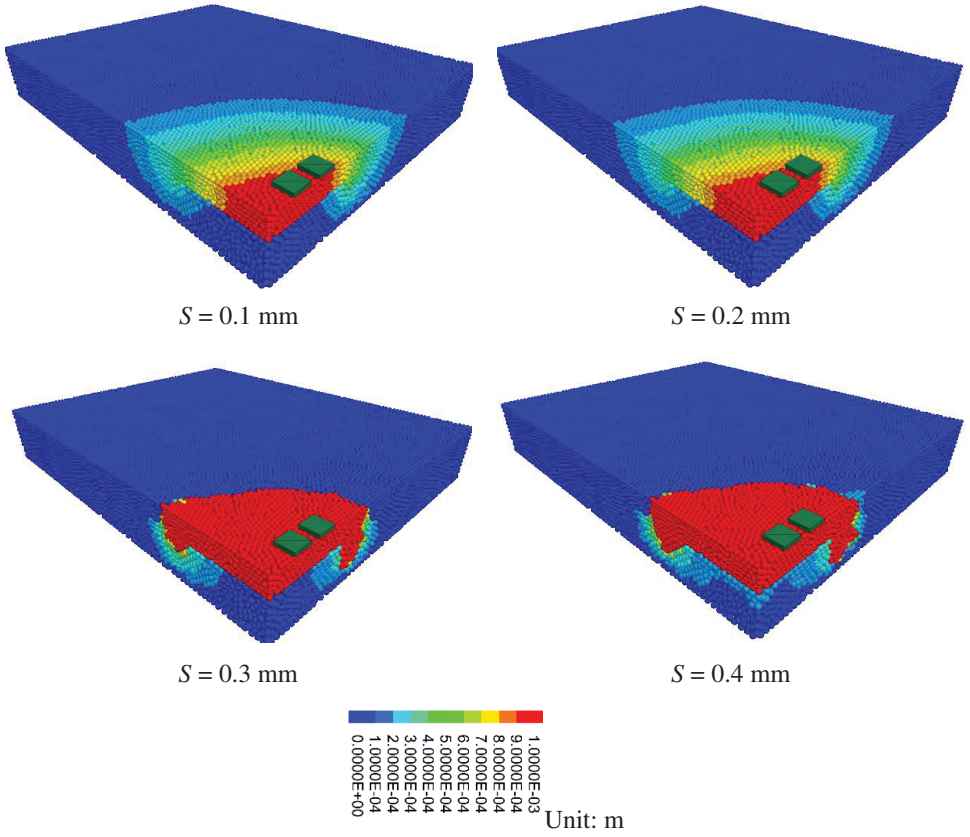

Figure 10: Displacement contour plot of the pavement slab corner void under loading

The crack distribution in the pavement slab corner void under loading is shown in Fig. 11. From the figure, it is clear that under corner detachment loading, the cracks are mainly divided into two parts. The first part: cracks begin beneath the loading plate and extend outward. The formation of this crack is mainly due to the pressure applied by the loading plate. When the load is applied, the concrete beneath the loading plate first experiences stress, and when the stress exceeds the tensile strength of the concrete, cracks will form. These cracks then propagate outward in the direction of stress transmission. The second part: arc-shaped shear bands form on both sides of the detachment region and extend downward. This is because the presence of the detachment area alters the load transfer path. On both sides of the detachment area, stress concentration is more intense, resulting in the formation of arc-shaped shear bands. These shear bands are formed as a result of concrete failure under shear stress, and as the load increases, the shear bands gradually extend downward. The formation mechanism of the first part of the cracks is primarily related to the tensile strength of concrete. Beneath the loading plate, the concrete experiences vertical pressure and tensile stress in the horizontal direction. When the tensile stress surpasses the tensile strength of the concrete, cracks will form. The direction of these cracks' extension aligns with the direction of the tensile stress, extending outward from beneath the loading

plate. The formation mechanism of the second part of the cracks is closely tied to shear stress. Due to the detachment area, stress concentration occurs on both sides of the detachment area during the load transfer process. In these areas, when the shear stress exceeds the shear strength of the concrete, shear bands will form. The arc-shaped shear band shape is determined by the distribution characteristics of the load at the edges of the detachment area, and the shear bands extend downward as shear failure develops with increasing load.

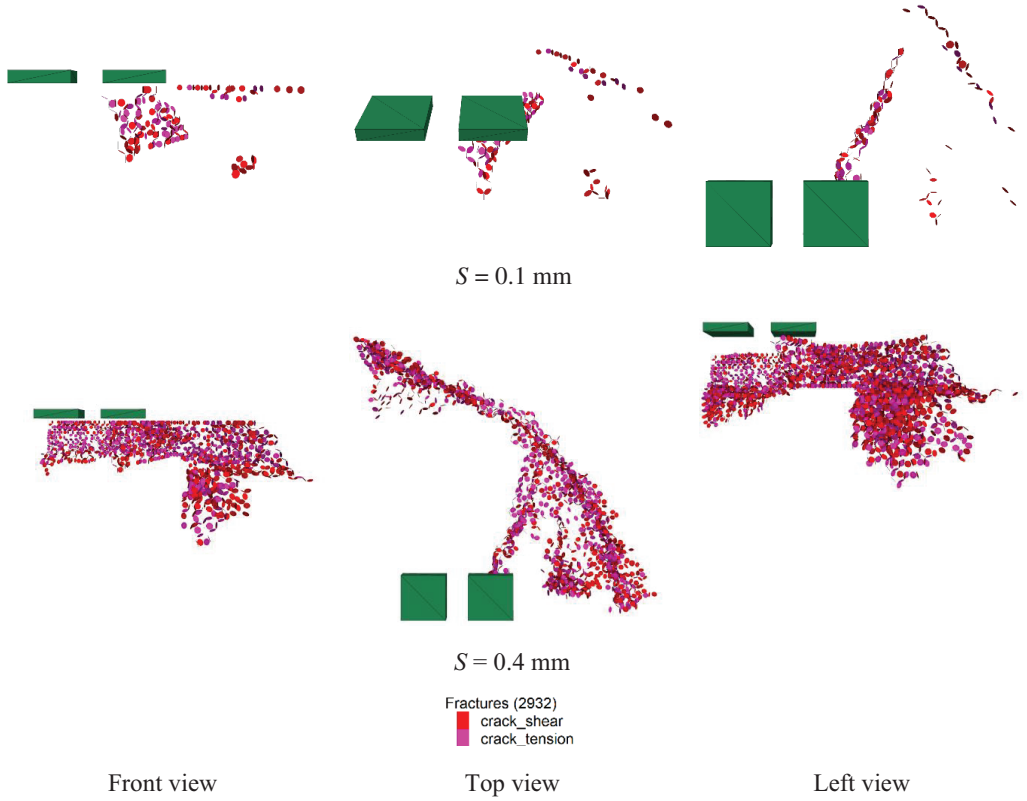

Figure 11: Crack distribution in the pavement slab corner void under loading

The displacement contour plot of the subgrade layer in the pavement slab corner void under loading is shown in Fig. 12. From the figure, it can be seen that in the case of corner detachment, the load bypasses the detachment area and is transmitted to the shear band region. This is because the detachment area cannot support the load, so during load transfer, the load seeks a path that can provide support. When the load bypasses the detachment area, it will concentrate in the shear band region, resulting in higher stress in this area. The stress concentration in the shear band region causes the material in this area to undergo significant deformation, resulting in larger settlement. The settlement pattern caused by this load transfer is consistent with the crack distribution pattern. In concrete structures, cracks generally initiate and propagate in regions with concentrated stress. When the load bypasses the detachment area and is transmitted to the shear band region, the shear band region undergoes significant settlement, and due to stress concentration, microcracks within the material gradually form and extend. As the load increases, both the number and length of cracks continue to increase, eventually forming a clear shear failure zone.

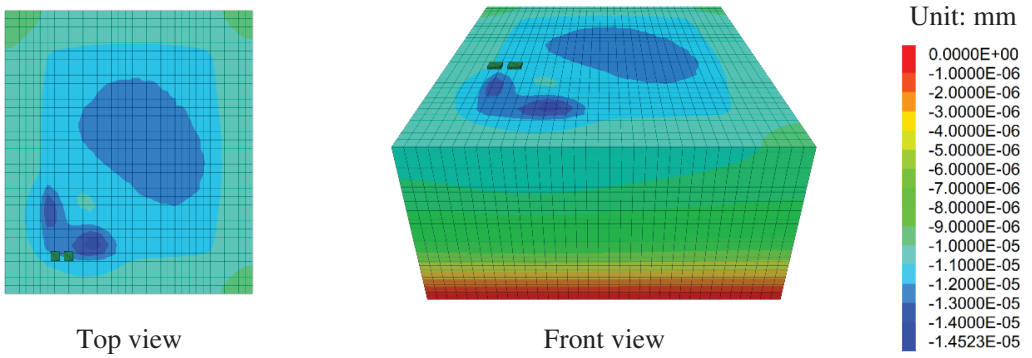

Figure 12: Displacement contour plot of the subgrade layer in the pavement slab corner void under loading (S = 4 mm)

A force chain refers to the pathway of force transmission between particles, while a strong force chain is the primary path for force transfer. Fig. 13 shows the force chain distribution in the pavement slab corner void under loading. From the figure, it can be seen that under corner detachment loading, the strong force chain primarily distributes along the fracture surface and beneath the load. This distribution pattern is similar to the crack distribution. The strong force chain is the primary path for force transfer between particles, and its distribution reflects the load transfer pathway inside the material. In the case of corner detachment, the presence of the detachment area changes the load transfer path, leading to the concentration of the strong force chain at the fracture surface and beneath the load. Cracks usually form and propagate in regions with concentrated stress. When the load is applied to the concrete surface layer, since the detachment area cannot bear the load, the load is transferred through the surrounding particles, forming a strong force chain. These strong force chains concentrate at the fracture surface and beneath the load, resulting in significant stress, and when the stress surpasses the material's strength limit, cracks form. As a result, the distribution of the strong force chain shows similarity with the crack distribution.

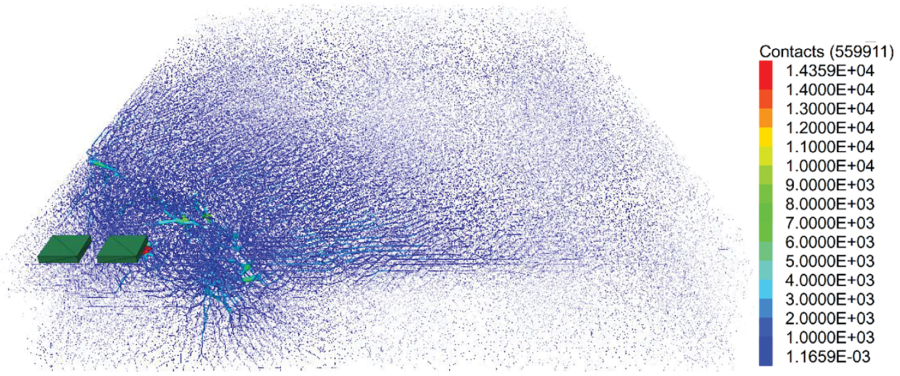

Figure 13: Force chain distribution in the pavement slab corner void under loading

Fig. 14 presents the relationship curve of the crack number vs. displacement. From the perspective of the curve shape and data distribution, in the stage where the displacement is within the first 0.1 mm, the crack number always remains at a level of 0. This phenomenon strongly indicates that, within this displacement interval, the internal structure of the concrete panel has not suffered damage and is in an

initial state of being intact and undamaged. The mechanical properties of the material itself can ensure its structural stability, and the externally applied displacement load has not yet induced the initiation of internal cracks. When the displacement exceeds the threshold of 0.1 mm, the crack number shows an extremely significant and rapid growth trend. This means that once the displacement surpasses this critical value, the internal structural balance of the concrete panel is broken, micro-cracks start to initiate in large numbers and expand rapidly, and the panel immediately enters the damage stage. As the number of cracks increases sharply, the stress transfer path inside the material is severely damaged, and the effective bearing area continuously decreases. This further leads to a rapid reduction in the panel strength and a sharp deterioration in mechanical properties. In the subsequent stage, the growth trend of the crack number gradually slows down. This is because, as the displacement continues to increase, a large number of cracks inside the panel keep expanding and intersecting, and finally form a penetrating failure. At this time, the crack expansion has tended to be "saturated" at the macroscopic level, and the space for newly initiated cracks is gradually restricted. Naturally, the growth of the crack number slows down. The concrete panel also loses most of its bearing capacity due to the penetrating failure, and the mechanical response enters a stable stage of residual deformation and damage development. The overall curve clearly shows the evolution of the entire process of the mechanical behavior of the concrete panel, from the initial intact state, through crack initiation and expansion, to penetrating failure. It provides an intuitive and crucial mesoscopic basis for deeply understanding its damage mechanism under load.

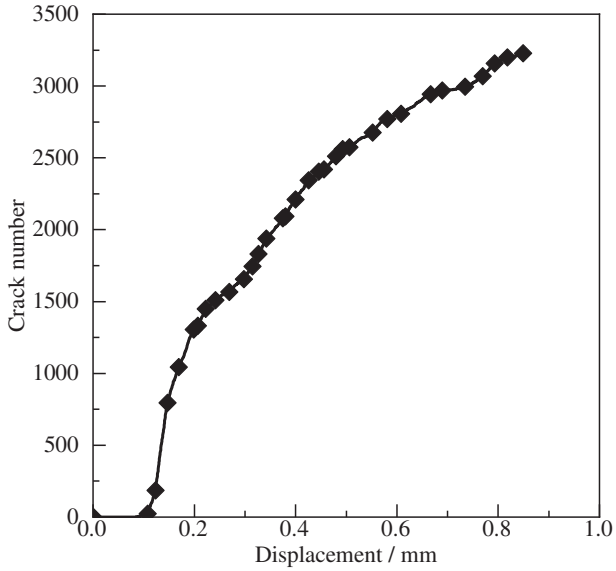

Figure 14: The curve of the crack number vs. displacement

The curve in the figure illustrates the variation law of the contact number with displacement (Fig. 15). In the initial loading stage (when displacement starts to increase from 0), the contact number shows a significant and rapid downward trend. This is because under the action of load, the internal stress of the concrete pavement slab continuously accumulates. When the stress concentration reaches a certain level, micro-cracks begin to initiate and propagate. The occurrence of these cracks destroys the originally stable contact state between internal particles and structural layers of the concrete, resulting in a sharp reduction in the effective contact number. As the displacement continues to increase, the decreasing trend of the contact number gradually becomes gentle. The mechanical mechanism behind

this phenomenon is that after a large number of cracks are generated in the early stage, the internal damage of the concrete pavement slab has developed to a certain extent, and the overall structure gradually enters a relatively "fragmented" stable damage stage. At this time, although the displacement is still increasing, the influence of newly generated cracks on the contact number is weakened. On one hand, the existing crack network restricts the unrestrained expansion of new cracks; on the other hand, the contact relationship of the remaining structure after concrete fragmentation is less sensitive to displacement changes compared with the initial damage stage. Thus, the decreasing rate of the contact number gradually slows down, showing the characteristic of a reduced curve slope and a gentler decreasing trend.

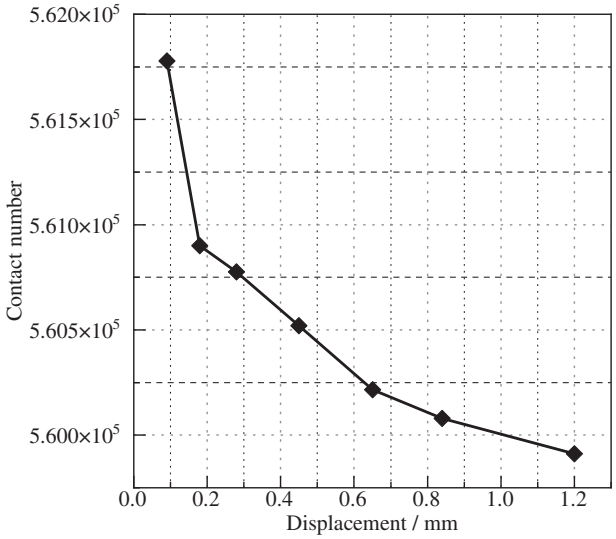

Figure 15: The curve of the contact number vs. displacement

The figure illustrates the variation law of contact force with displacement under different prefabricated crack thicknesses (Fig. 16). Overall, all three curves show a trend of first rapidly rising to a peak and then fluctuating downward, but the difference in prefabricated crack thickness significantly affects the curve characteristics. As the prefabricated crack thickness increases from 1 cm to 2 cm and then to 3 cm, the peak strength gradually decreases. Specifically, when H = 3 cm, the peak load is approximately 56 kN; compared with the case of H = 1 cm, the reduction amplitude of the peak load is about 71%; while for H = 2 cm, the reduction amplitude of the peak load is about 35%. Notably, as the prefabricated crack thickness increases, the decreasing trend of the peak strength is not uniform but shows a characteristic of "first rapid and then gentle"-from H = 1 to H = 2 cm, the reduction amplitude is relatively large; from H = 2 to H = 3 cm, the reduction amplitude decreases, that is, the decreasing trend of the peak strength slows down.

From the perspective of mechanical mechanism analysis, the prefabricated crack thickness can be analogously regarded as reflecting the degree of voiding in the concrete pavement slab (the larger the crack thickness, the more significant the voiding). In the initial loading stage, the voided area will change the internal stress transfer path of the slab, intensifying the stress concentration phenomenon. When the voiding degree is small (such as from H = 1 to H = 2 cm), the structural stiffness decreases significantly, and the bearing capacity is more sensitive to the change of voiding, so the peak load has a large reduction amplitude; as the voiding degree further increases (such as from H = 2 to H = 3 cm), a certain degree of damage has accumulated inside the slab, and the "response threshold" of the

remaining effective bearing structure to the load increases, and the marginal effect of voiding on the peak strength weakens, resulting in a slower decreasing trend of the peak strength.

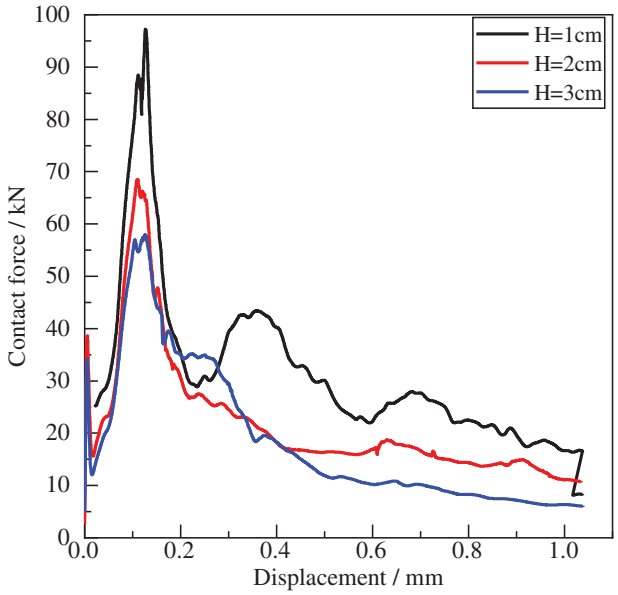

Figure 16: The variation law of contact force with displacement under different prefabricated crack thicknesses

3.2 Model Development and Loading Analysis of Grouting-Reinforced Pavement Slab Corner Void

The reinforcement method using generated particles to fill the detachment areas of the bottom plate and corner area is adopted. This method implements grouting reinforcement by injecting small-radius particles into the detachment areas. The particle size in the reinforced region is 0.5 mm, with a total of 9800 particles. The smaller particle size helps better fill the voids in the detachment area, improving the filling efficiency. The fundamental principle of grouting reinforcement is to use the injected particles to fill the detachment areas, forming a new supporting structure that increases the load-bearing capacity and stability of the structure. The injected particles interact within the detachment area, forming a reinforced region with a certain strength. The final FEM-DEM coupled model of the reinforced pavement slab corner under loading is shown in Fig. 17. The mesoscopic parameters of the grouting reinforcement area are shown in Table 5.

Fig. 18 shows the load vs. displacement relationship and microcrack evolution in the reinforced pavement slab corner under loading. In the case of corner reinforcement, the peak occurs at a displacement of 0.12, with a peak strength of 150 kN. Compared to corner detachment, the peak strength of the reinforced corner increased by 53%. The displacement is in the elastic phase until 0.08 mm, with the crack initiation pressure at 75 kN. This suggests that the reinforced corner structure begins to develop microcracks under relatively low loads. After reaching the initiation pressure, the cracks rapidly grow and then stabilize. This indicates that in the reinforced corner structure, once microcracks form, they quickly expand, and then, due to the redistribution of internal stresses, the number of cracks remains relatively stable.

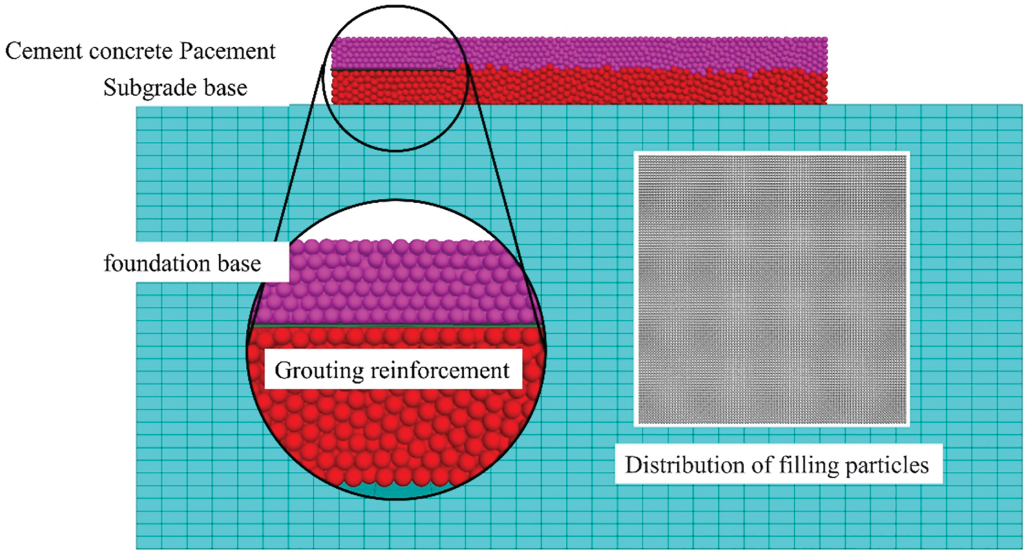

Figure 17: FEM-DEM coupled model of the reinforced pavement slab corner under loading

Table 5: Mesoscale parameters for grouting reinforcement area

Different strata	Grouting reinforcement area
Particle contact model	Linearpbond
Effective modulus (Pa)	50e9
Normal-to-shear stiffness ratio	1
Bond effective modulus (Pa)	50e9
Bond normal-to-shear stiffness ratio	1
Tensile strength (N)	15e6
Cohesion (N)	15e6
Friction angle (°)	0
Friction coefficient	0.5
Particle density (kg/m^3)	2800

From the displacement contour map under corner reinforcement loading, the failure mode appears rectangular (Fig. 19). This rectangular failure mode contrasts with the triangular failure mode observed in the case of central reinforcement. The rectangular failure mode suggests that under corner reinforcement, the load transfer and stress distribution exhibit unique features. The stress concentration in the reinforced corner area under loading causes this rectangular failure mode. Due to the occurrence of the rectangular failure mode, the depth of the damage is typically greater. This is because the rectangular shape enables stress to be transferred more deeply in the vertical direction, resulting in deeper structural damage. The failure mode of central reinforcement is triangular, whereas the failure mode under corner reinforcement is rectangular. Triangular failure usually indicates that stress is concentrated in a more localized area, whereas rectangular failure indicates that stress is more evenly distributed across a broader area. The rectangular failure mode under corner reinforcement has

a greater depth, which may be due to the fact that the corner reinforcement design does not consider the stress diffusion mechanism as central reinforcement does, leading to deeper vertical load transmission and consequently deeper damage.

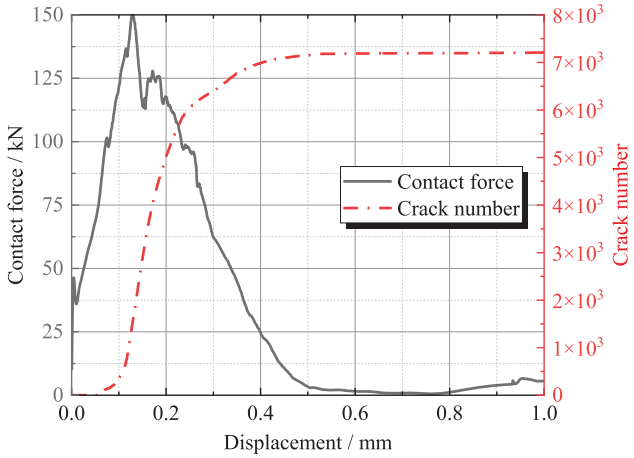

Figure 18: Load vs. displacement and microcrack evolution in the reinforced pavement slab corner under loading

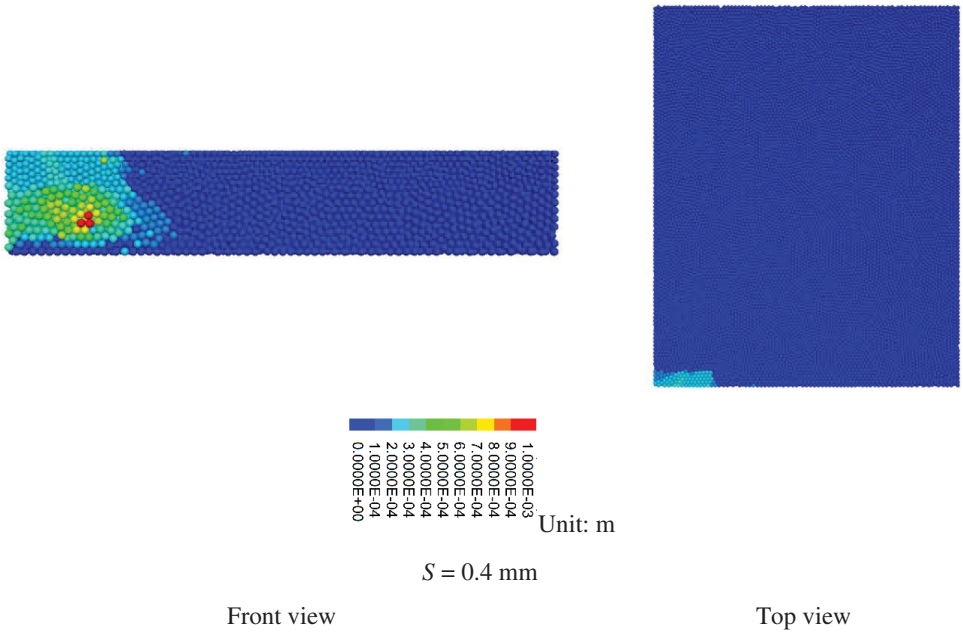

Figure 19: Displacement contour plot of the reinforced pavement slab corner under loading

From the crack distribution diagram after reinforcement and loading (Fig. 20), it can be seen that during corner loading, the structure experiences significant stress in localized areas, resulting in rapid crack expansion. The failure mode resembles that of bottom slab detachment, exhibiting a semicircular distribution. This semicircular failure mode is typically related to shear stress. Under corner loading conditions, the shear stress inside the structure leads to crack propagation along a semicircular path.

The failure is predominantly shear-related, indicating that under these loading conditions, the internal shear stress exceeds the material's shear strength, resulting in shear failure. Shear failure usually reduces the structural integrity, thereby impacting the structure's load-bearing capacity. When a load is applied to the corner, it propagates through the structure, resulting in stress concentration near the loading zone. The unique nature of corner loading causes uneven stress distribution within the structure, with shear stress peaking in certain areas. The semicircular failure mode arises from the shear stress transmission path within the structure. Shear stress propagates from the loading point to the surrounding areas, leading to cracks expanding along a semicircular path and forming a characteristic semicircular failure mode.

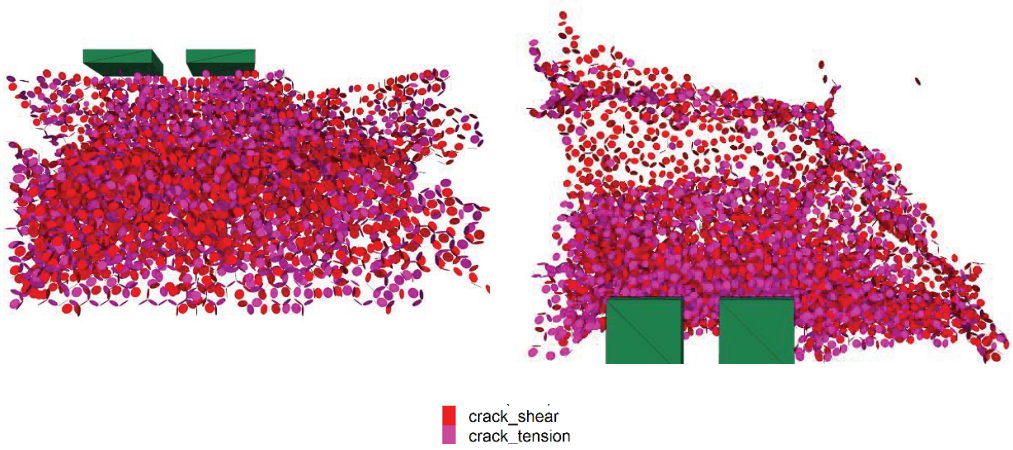

Figure 20: Crack distribution in the reinforced pavement slab corner under loading (S = 0.4 mm)

From the foundation displacement contour map after reinforcement (Fig. 21), it is observed that the load is transmitted to the foundation through the corners of the loading plate, and the load distribution is relatively scattered, resulting in a smaller maximum displacement.

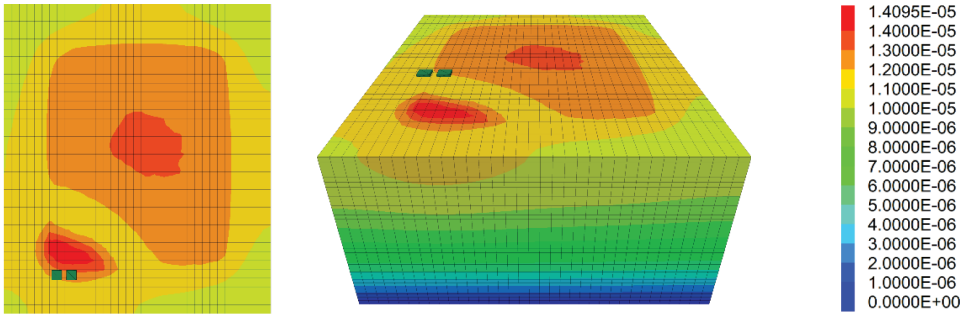

Figure 21: Displacement contour plot of the subgrade layer in the reinforced pavement slab corner under loading

The force chain distribution in the reinforced pavement slab corner under loading is shown in Fig. 22. From the side loading force chain distribution map after reinforcement, it is observed that the force chain shows a downward transmission trend, primarily distributed in the concrete surface layer. This suggests that in the case of corner loading, the load is transmitted through the concrete surface layer. The force chain exhibits a semi-circular distribution, which is typically associated with the load transfer path and the stress distribution of the structure. When corner loading is applied, the load creates a semi-circular stress distribution region within the concrete surface layer, causing the force chain to exhibit a corresponding semi-circular distribution. When the load is applied at the corner, it first acts on the concrete surface layer. Because of the high compressive strength of concrete, the load is transferred within the surface layer through the interaction between particles (i.e., the force chain). The semi-circular distribution of the strong force chain reflects the transmission path of the load within the concrete surface layer. The load spreads from the loading point to the surrounding area, creating a semi-circular stress distribution region, which causes the force chain to concentrate in that region.

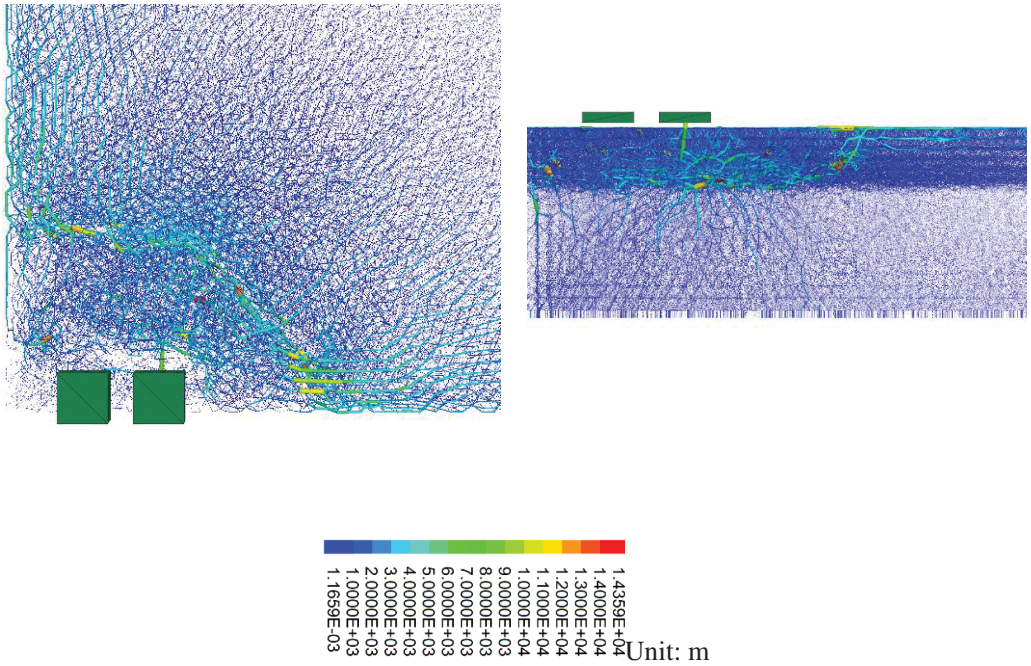

Figure 22: Force chain distribution in the reinforced pavement slab corner under loading

An analysis of the data in Table 6 reveals the following insights into the performance of the concrete panel before and after grouting reinforcement. The peak strength of the panel increased significantly from 97.2 to 150 after grouting, indicating that the reinforcement effectively improved the internal structure of the concrete and enhanced its load-bearing capacity. This improvement allows the panel to withstand higher stresses before failure, thereby enhancing the overall compressive performance of the structure. The displacement at peak strength remained unchanged at 0.12 before and after grouting, suggesting that the reinforcement did not alter the deformation characteristics of the panel when reaching its peak strength. This implies that the degree of deformation at the instant of reaching the ultimate strength remained consistent, indicating stable deformation behavior

of the material. The number of cracks at peak strength increased dramatically from 25 to 1188 after grouting. This increase does not necessarily indicate a reduction in crack resistance but rather reflects changes in the stress distribution and transfer mechanisms within the material due to the reinforcement. The grouting process likely led to the formation and detection of more microcracks as the material's enhanced strength allowed it to redistribute stress more effectively. This transformation from a few macroscopic cracks to numerous microcracks may help disperse stress and prevent the rapid propagation of single large cracks, which could otherwise lead to structural failure. This phenomenon indirectly demonstrates that grouting optimizes the stress-bearing system of the panel. In summary, grouting reinforcement significantly improves the peak strength of the concrete panel and optimizes the crack distribution and stress transfer during loading. Although the displacement characteristics at peak strength remain unchanged, the enhancements in strength and crack behavior indicate that grouting effectively enhances the mechanical properties and structural stability of the concrete panel, making it a valuable technique for the reinforcement and maintenance of such structures.

Table 6: Comparison of concrete panel results before and after grouting reinforcement

State	Peak strength (kN)	Displacement at peak strength (kN)	Number of cracks at peak strength (kN)
Before grouting	97.2	0.12	25
After grouting	150	0.12	1188

4 Discussion

Discussion on the Limitations of FEM-DEM: FEM relies on macroscopic constitutive parameters (e.g., Young's modulus, Poisson's ratio), while DEM depends on mesoscopic parameters (particle stiffness, friction coefficient). The two lack a theoretical correlation, requiring empirical calibration that leads to a loss of accuracy. The discrete nature of particles and the continuity of FEM meshes cause geometric incompatibility at contact boundaries, resulting in distortion in force transmission and non-physical oscillations.

This study explored the strength change of concrete panels before and after grouting via FEM-DEM coupled simulation, providing a reference for engineering practice. The model was set with homogeneous materials based on the characteristics of the FEM-DEM coupling method to ensure simulation stability and operability, facilitating focus on the core impact of grouting on strength. Static loading was adopted for two reasons: firstly, dynamic loading reduces the computational efficiency of discrete elements and increases time cost; secondly, preliminary verification shows that for the strength change issue concerned in this study, results of the two loading modes are consistent. Thus, static loading can ensure conclusion reliability while improving efficiency. This study has limitations: it does not deeply involve practical factors such as dynamic traffic loads, environmental effects and imperfect grouting. Future research will investigate the impact of different grouting degrees on the peak strength of panels and combine the above practical factors to improve the model, enhancing the engineering applicability of the results.

5 Conclusions

This paper systematically studies the mechanical characteristics of concrete pavement corner detachment and post-grouting reinforcement based on the FEM-DEM coupling method, and the following main conclusions are obtained:

The mesoscopic parameters of the concrete surface layer and the base course are calibrated through uniaxial compression simulation, and an FEM-DEM coupling numerical model of the pavement structure with corner detachment is established. This model can effectively simulate the macro and mesoscopic mechanical behaviors after corner detachment and post-grouting reinforcement, providing a powerful tool for subsequent research.

In the case of corner detachment, the cracking load is 75 kN and the peak load is 96.8 kN. After the load exceeds the peak value, the number of cracks increases rapidly; when the strain reaches 0.2, the growth trend of cracks slows down. The displacement area expands in a triangular shape from under the load plate to the surrounding area. The failure mode is shear failure, and the cracks are divided into two parts: one part extends outward from under the load plate, and the other part is an arc-shaped shear band that extends downward on both sides of the detachment area. The load bypasses the detachment area and is transmitted to the shear band area. The strong force chains are mainly distributed on the fracture surface and under the load, which is similar to the crack distribution. The crack number-displacement curve shows that cracks initiate at a displacement of 0.1 mm, then grow rapidly until penetrating failure slows the growth rate, fully presenting the entire process of the concrete panel from initially intact to damaged and failed.

After the corner grouting reinforcement, the peak strength is increased by 53% to reach 150 kN. The displacement is in the elastic stage until it reaches 0.08 mm, and the cracking pressure is 75 kN. After the cracks reach the cracking pressure, they increase rapidly first and then remain stable. The failure form is rectangular, with a relatively large failure depth. The crack distribution is semi-circular, and the failure is mainly shear failure. The load is transmitted to the foundation through the corners of the plate, with a relatively scattered distribution and a small maximum displacement. The force chains are transmitted downward and mainly distributed in the concrete surface layer, and the strong force chains are semi-circularly distributed.

The research results reveal the change rules of the mechanical characteristics of concrete pavement corner detachment and post-grouting reinforcement, providing a theoretical basis for the research of grouting treatment methods for concrete pavement corner detachment, and are of great significance for guiding the prevention and treatment of pavement diseases in practical engineering.

Acknowledgement: This work was supported by the Guizhou Communications Polytechnic University. We gratefully acknowledge the Guizhou Minzu University and Changjiang River Scientific Research Institute for providing the necessary equipment for this study. We would like to thank Dr. Wang for his technical assistance during the experiments.

Funding Statement: This work had been supported by the Fund Project: the Yongjiang Program for Young Talents of Nanning Science and Technology Bureau (RC20230204); the Science and Technology Project of Guizhou Province (Qiankehe Fundamental QN[2025]420); Science and Technology Project of Guizhou Provincial Department of Transport (2025-121-015); the National Natural Science Foundation of China (52268054); the Natural Science Foundation of Guizhou Minzu University (GZMUZK[2023]CXTD04); Basic Research Project of Guizhou Provincial Department of Science and Technology, China (Grant No. ZK [2021]-290); Science and Technology Project of Guizhou

Provincial Department of Transport, China (Grant No. 2023-123-036); Guizhou Province Science and Technology Plan Project, China (Grant No. GZSTCPT-CXTD[2021]008); Key Laboratory of High Performance Restoration Materials for Higher Education Construction Projects in Guizhou Province, China (Grant No. [2023]030).

Author Contributions: The authors confirm contribution to the paper as follows: study conception and design: Xiaoyong Zhang, Baoyin Mei; data collection: Jianxue Feng, Tiancheng Wang; analysis and interpretation of results: Deqiang Chen; draft manuscript preparation: Xiaoyong Zhang. All authors reviewed the results and approved the final version of the manuscript.

Availability of Data and Materials: Due to the nature of this research, participants of this study did not agree for their data to be shared publicly, so supporting data is not available.

Ethics Approval: Not applicable.

Conflicts of Interest: The authors declare no conflicts of interest to report regarding the present study.

References

1. Li J, Zhang W, Cao Y. Laboratory evaluation of magnesium phosphate cement paste and mortar for rapid repair of cement concrete pavement. Constr Build Mater. 2014;58(2):122–8. doi:10.1016/j.conbuildmat.2014.02.015.
2. Shi X, Mukhopadhyay A, Zollinger D. Sustainability assessment for portland cement concrete pavement containing reclaimed asphalt pavement aggregates. J Clean Prod. 2018;192(1):569–81. doi:10.1016/j.jclepro.2018.05.004.
3. Rudnicki T, Stałowski P. Fast-setting concrete for repairing cement concrete pavement. Materials. 2023;16(17):5909. doi:10.3390/ma16175909.
4. Luo Y, Luo Y, Wu C, Yussof MM. Finite element simulation and falling ball impact model for cement concrete pavement considering void under slab. Constr Build Mater. 2024;427(10):136245. doi:10.1016/j.conbuildmat.2024.136245.
5. Ali S, Fawzia S, Thambiratnam D, Liu X, Remennikov A. Performance of protective concrete runway pavement under aircraft impact loading. Struct Infrastruct Eng. 2020;16(12):1698–710. doi:10.1080/15732479.2020.1730405.
6. Gu H, Jiang X, Li Z, Yao K, Qiu Y. Comparisons of two typical specialized finite element programs for mechanical analysis of cement concrete pavement. Math Probl Eng. 2019;2019(1):9178626. doi:10.1155/2019/9178626.
7. Xie N, Akin M, Shi X. Permeable concrete pavements: a review of environmental benefits and durability. J Clean Prod. 2019;210(2):1605–21. doi:10.1016/j.jclepro.2018.11.134.
8. Fotiadi A, Gnezdilova S, Strekha I. Remote method for predicting damage to cement concrete pavements. In: International Scientific Conference on Innovations and Technologies in Construction. Cham, Switzerland: Springer International Publishing; 2020. p. 333–9.
9. Roesler J, Khazanovich L. Finite-element analysis of portland cement concrete pavements with cracks. Transport Res Rec. 1997;1568(1):1–9. doi:10.3141/1568-01.
10. Xu C, Cebon C. Foundation voiding in jointed plain concrete pavements. J Eng Mech. 2017;143(6):04017018. doi:10.1061/(ASCE)EM.1943-7889.0001209.
11. Ao X, Wang X, Zhu X, Zhou Z, Zhang X. Grouting simulation and stability analysis of coal mine goaf considering hydromechanical coupling. J Comput Civ Eng. 2017;31(3):04016069. doi:10.1061/(ASCE)CP.1943-5487.0000640.

12. Sun Y, Li G, Zhang J, Qian D. Stability control for the rheological roadway by a novel high-efficiency jet grouting technique in deep underground coal mines. Sustainability. 2019;11(22):6494. doi:10.3390/su11226494.
13. Zhao T, Liu C. Roof instability characteristics and pre-grouting of the roof caving zone in residual coal mining. J Geophys Eng. 2017;14(6):1463–74. doi:10.1088/1742-2140/aa8eb6.
14. Lu G, Wang YS, Zhang Y, Ariaratnam ST. Feasibility of using sodium silicate as grouting in loose coal bed sections for methane drainage. Tunnelling Undergr Space Technol. 2018;72:107–13. doi:10.1016/j.tust.2017.11.011.
15. Liang K, Zeng X, Ali S. Hydrodynamic pressure distribution in saturated void beneath cement concrete pavement slab. Int J Pavement Eng. 2020;3(5):1–9. doi:10.1080/10298436.2020.1804064.
16. Cundall P, Hart R. Numerical modelling of discontinua. Eng Comput. 1992;9(2):101–13. doi:10.1108/eb023851.
17. Pei Z, Yi J, Mao Q, Feng D, Wang D. DEM analysis of the evolution of reflection cracks in old cement concrete pavement with an ATB layer. Int J Pavement Eng. 2023;24(2):2049263. doi:10.1080/10298436.2022.2049263.
18. Vaddy P, Pandurangan V, Biligiri K. Discrete element method to investigate flexural strength of pervious concrete. Constr Build Mater. 2022;323(7315):126477. doi:10.1016/j.conbuildmat.2022.126477.
19. Xie S, Yi J, Wang H, Yang S-H, Xu M, Feng D. Mechanical response analysis of transverse crack treatment of asphalt pavement based on DEM. Int J Pavement Eng. 2022;23(7):2206–26. doi:10.1080/10298436.2020.1849687.
20. Zhu H, Wei G, Xu H, Yu X, Ma D. The influence of interlayer bonding conditions on the propagation laws of reflective cracks in semi-rigid base pavement based on the DEM and GPR. Constr Build Mater. 2024;442:137547. doi:10.1016/j.conbuildmat.2024.137547.
21. Meng D, Lei W, Han J, Li H, Huang Y. Research on the effects of pit excavation on adjacent existing subway tunnel structures based on the FEM-DEM coupling method. Métodos Numéricos Para Cálculo Y Diseño En Ingeniería: Revista Internacional. 2024;40(3):8. doi:10.23967/j.rimni.2024.10.57763.
22. Jin D, Guo Y, Li X, Yuan D, Shu J, Chen J, et al. Modeling of reinforced-concrete cutting with shield rippers using FEM-DEM-coupling method. Int J Mech Sci. 2024;282(10):109619. doi:10.1016/j.ijmecsci.2024.109619.
23. Ge H, Quezada JC, Le Houerou V, Chazallon C, Sha A. From macro to micro: investigation of three-dimensional particle-scale responses of asphalt mixtures under non-uniform rolling tire loads via coupled FEM-DEM simulations. Road Mater Pavement Des. 2025;2025(3):1–30. doi:10.1080/14680629.2025.2478617.
24. Feng J, Luo R, Dong X, Zhang X, Shen Q. Performance of monotonic pile penetration in sand: model test and DEM simulation. Buildings. 2024;14(10):3327. doi:10.3390/buildings14103327.
25. Li L, Zheng M, Liu X, Wu W, Liu H, Hesham El Naggar M, et al. Numerical analysis of the cyclic loading behavior of monopile and hybrid pile foundation. Comput Geotech. 2022;144(6):104635. doi:10.1016/j.compgeo.2022.104635.
26. Li L, Wu W, Jiang G, El Naggar MH, Liu X, Liao K, et al. Discrete-continuum modelling on the bearing mechanism of pile-bucket foundation under static lateral load. Ocean Eng. 2025;318(11):120149. doi:10.1016/j.oceaneng.2024.120149.
27. Chen Q, Li Z, Dai Z, Wang X, Zhang C, Zhang X. Mechanical behavior and particle crushing of irregular granular material under high pressure using discrete element method. Sci Rep. 2023;13(1):7843. doi:10.1038/s41598-023-35022-w.
28. Hu Z, Xie L, Qin Y, Liu X, Qian J. Numerical simulation of size effect of defective rock under compression condition. Sci Rep. 2023;13(1):420. doi:10.1038/s41598-023-27651-y.

29. Zhang X, Luo K, Wang T, Jiang M, Feng J, Mei G. Microscopic mechanism of coarse-grained soil under triaxial test based on PFC-FLAC coupling method. Soil Mech Found Eng. 2023;60(4):323–9. doi:10.1007/s11204-023-09897-w.
30. Fang J, Lin S, Liu K. Multi-scale study of load-bearing mechanism of uplift piles based on model tests and numerical simulations. Sci Rep. 2023;13(1):6410. doi:10.1038/s41598-023-33221-z.
31. Zhang X, Wang T, Zhao C, Jiang M, Xu M, Mei G. Supporting mechanism of rigid-flexible composition retaining structure in sand ground using discrete element method. Comput Geotech. 2022;151(3):104967. doi:10.1016/j.compgeo.2022.104967.
32. Zhang X, Jiang M, Yang J, Zhao C, Mei G. The macroscopic and mesoscopic study on strengthening mechanisms of the single pile with raft under pile-soil-raft combined interaction. Comput Geotech. 2022;144(4):104630. doi:10.1016/j.compgeo.2021.104630.